Dalton Transactions

PAPER

View Article Online
View Journal

Cite this: DOI: 10.1039/c5dt01796c

Biomimetic peptide-based models of [FeFe]-hydrogenases: utilization of phosphine-containing peptides†

Souvik Roy,‡ Thuy-Ai D. Nguyen,§ Lu Gan and Anne K. Jones*

Received 13th May 2015,
Accepted 23rd July 2015

DOI: 10.1039/c5dt01796c

www.rsc.org/dalton

Two synthetic strategies for incorporating diiron analogues of [FeFe]-hydrogenases into short peptides *via* phosphine functional groups are described. First, utilizing the amine side chain of lysine as an anchor, phosphine carboxylic acids can be coupled *via* amide formation to resin-bound peptides. Second, artificial, phosphine-containing amino acids can be directly incorporated into peptides *via* solution phase peptide synthesis. The second approach is demonstrated using three amino acids each with a different phosphine substituent (diphenyl, diisopropyl, and diethyl phosphine). In total, five distinct monophosphine-substituted, diiron model complexes were prepared by reaction of the phosphine-peptides with diiron hexacarbonyl precursors, either $(\mu\text{-pdt})Fe_2(CO)_6$ or $(\mu\text{-bdt})Fe_2(CO)_6$ (pdt = propane-1,3-dithiolate, bdt = benzene-1,2-dithiolate). Formation of the complexes was confirmed by UV/Vis, FTIR and ^{31}P NMR spectroscopy. Electrocatalysis by these complexes is reported in the presence of acetic acid in mixed aqueous-organic solutions. Addition of water results in enhancement of the catalytic rates.

Introduction

Hydrogenases, the biological catalysts for the reversible reduction of protons to molecular hydrogen, employ earth-abundant base metals, either iron or nickel and iron, to carry out this transformation under mild conditions.[1] The utility of this reaction for developing technologies to produce sustainable solar fuels has engendered widespread interest in [FeFe]-hydrogenases, the most efficient biological system for producing hydrogen. X-ray crystallographic studies revealed that the structure of the active site of [FeFe]-hydrogenase, known as the H-cluster, consists of a [2Fe] subsite covalently connected to a [4Fe4S] cubane.[2] The H-cluster is connected to the protein *via* only a single cysteinyl thiolate, which also bridges the [4Fe4S] cubane and the [2Fe] subsite (Scheme 1A). The [2Fe] subsite features CO and CN^- as terminal diatomic ligands and a biologically unusual non-proteinaceous dithiolate ligand bridges the two iron centers.

From a structural perspective, the [2Fe] subunit is reminiscent of the well-known organoiron complex $[(\mu\text{-pdt})Fe_2(CO)_6]$ (pdt = propane-1,3-dithiolate) which serves as a convenient starting point for building a multitude of sophisticated biomimetic diiron analogues.[3] Although many of these bio-inspired organometallic models show moderate electrocatalytic proton reduction activity, none of them catalyzes hydrogen production with the same exquisite combination of high turnover frequency and low activation energy as the enzymes.[4] Moreover, the hydrophobic nature of these diiron dithiolate clusters renders most of them soluble only in organic solvents. They are therefore unsuitable for applications in fuel cells employing aqueous solutions, and their activity in such a setting cannot be evaluated.

Recently, the importance of the protein environment for the catalytic activity of hydrogenases and other metalloenzymes has become increasingly clear.[5] For example, the

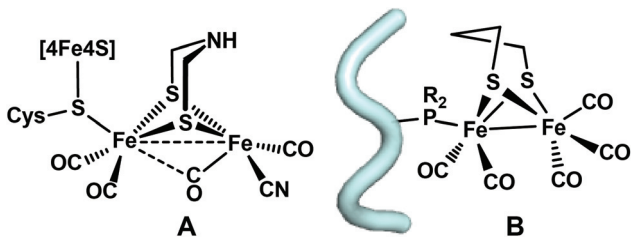

Scheme 1 (A) [FeFe]-hydrogenase active site (H-cluster) and (B) model representation of peptide-bound diiron complexes described in this study.

Department of Chemistry and Biochemistry, Arizona State University, Tempe, AZ 85287, USA. E-mail: jonesak@asu.edu; Tel: +1-480-965-0356

†Electronic supplementary information (ESI) available. See DOI: 10.1039/c5dt01796c

‡Current Address: Laboratory of Chemistry and Biology of Metals, CEA-Grenoble, 17 Rue des Martyrs, 38054 Grenoble Cedex-9, France.

§Current Address: Department of Chemistry and Biochemistry, University of California Santa Barbara, Santa Barbara, CA 93106, USA.

hydrogenase protein component has been shown to contribute to stabilization of the diiron site in a strained "rotated" structure that leaves one of the irons with an open coordination site thought to be essential for catalysis.[6] Additionally, starting from the apo-enzyme and a model diiron complex with virtually no catalytic activity, complete reconstitution of fully functional [FeFe]-hydrogenases has been achieved.[5b] This clearly demonstrates the importance of the protein environment for facilitating efficient, bidirectional catalysis and has spurred efforts to incorporate bio-inspired catalysts and hydrogenase models into supramolecular constructs to investigate the impact of secondary coordination sphere interactions on chemical properties and produce synthetic catalysts with greater activity.[7]

Designed protein and peptide models that bind natural or artificial metallocofactors are proving to be a powerful approach both for tuning the reactivity of embedded metallocenters and for probing the mechanisms of the metalloenzymes that have inspired them.[8] Small artificial peptides binding diiron hydrogenase models serve as bridges between natural metalloenzymes and organometallic analogues and present an opportunity to introduce secondary coordination sphere interactions into the models. Synthetic methods have been developed to incorporate thiolate bridged diiron hexacarbonyl clusters into suitably designed peptides *via* both natural cysteine and artificial dithiol groups.[9] However, these hexacarbonyl [FeFe]-hydrogenase models are less electron rich and thus poorer catalysts than pentacarbonyl complexes in which a terminal CO ligand is replaced by a stronger donor like a phosphine. Furthermore, substitution of one of the carbonyls in these peptide-based models is challenging because low yields result from the awkward solvent mixtures that are required to simultaneously solubilize both the peptide and the substituting ligand.

Phosphines have been widely employed in models as a surrogate for the CN^- ligand found in hydrogenases,[10] and construction of phosphine-functionalized peptides represents a tantalizing route to peptide-based diiron models with better electrocatalytic properties. Moreover, phosphino-peptides offer the possibility of synthesizing a wide range of ligands through variation of the peptide sequence as well as the substituents on the phosphines. In this report, we describe two general methods for introducing a phosphine functionality into small peptides. The first approach is to tether the phosphine to the side chain amine of a lysine within a resin-bound peptide. The second method is to incorporate a protected artificial phosphine amino acid directly into the peptide during solution phase peptide synthesis. To demonstrate the efficiency of the second synthetic approach, three amino acids were prepared with distinct substituents on the phosphines using the method developed by Gilbertson and co-workers: *N*-Boc-3-(diethylphosphorothioyl)alanine (Boc-Epa-OH), *N*-Boc-3-(diisopropylphosphorothioyl)alanine (Boc-Ipa-OH), and *N*-Boc-3-(diphenylphosphorothioyl)alanine (Boc-Ppa-OH).[11] Four diiron-peptide complexes were synthesized using these phosphine amino acids, and the influence of the peptide ligands on the hydrophilicity, redox properties and electrocatalytic activities of coordinated diiron carbonyl complexes were explored in acetonitrile and acetonitrile/water mixtures. Notably, the complexes display favorable energetics towards electrocatalytic proton reduction from acetic acid in the presence of water.

Results and discussion

Synthesis and characterization of the metallopeptides

We present two strategies to construct phosphine-functionalized artificial peptides. The first is analogous to our previous method for creating dithiol functionalized peptides. As shown in Scheme 2, using the amine side chain of a lysine as an anchor, a resin-bound peptide is modified *via* amide formation with a phosphine-containing, aliphatic carboxylic acid creating a phosphine-bearing lysine derivative. In the second approach, several phosphine-containing amino acids have been directly incorporated *via* solution-phase peptide synthesis. After synthesis, the phosphine-functionalized peptide can be reacted with diironhexacarbonyl complexes [(μ-SRS)-$Fe_2(CO)_6$] (R = organic group) in the presence of a decarbonylating agent (trimethylamine-*N*-oxide) resulting in substitution of one of the CO ligands by the phosphine.

On-resin modification of peptide. Scheme 2 outlines the approach for attaching a phosphine to a resin-bound peptide,

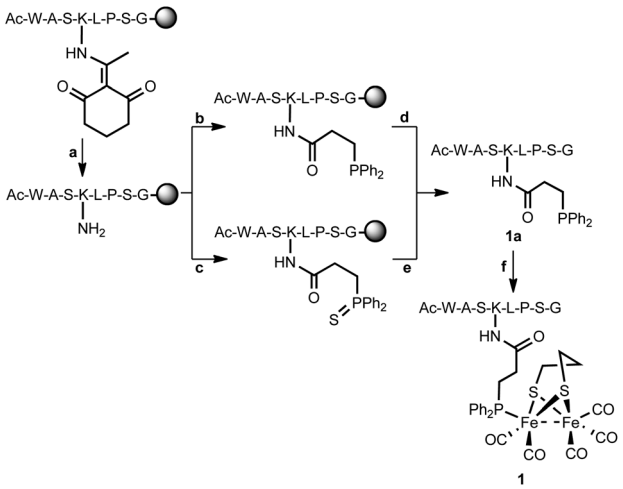

Scheme 2 Synthetic scheme for on-resin modification of the lysine residue of an eight amino acid peptide to incorporate a phosphine functional group and subsequent reaction with diiron-hexacarbonyl to produce the [(μ-pdt){$Fe(CO)_3$}{peptide-$Fe(CO)_2$}] complex (**1**). The protecting groups on all the amino acid residues except lysine remain intact until the peptide is cleaved from the resin. The overall yield of **1**, starting from the peptide synthesis, was approximately 5%. The sphere represents the resin bead. Reaction conditions: (a) 2% N_2H_4, DMF; (b) $Ph_2PC_2H_4COOH$, HATU, DIEA, DMF; (c) $Ph_2P(S)C_2H_4COOH$, HATU, DIEA, DMF; (d) 95% TFA, 2.5% water, 2.5% TIPS; (e) (i) 95% TFA, 2.5% water, 2.5% TIPS, (ii) Raney™ nickel, aq. CH_3CN; (f) (μ-pdt)$Fe_2(CO)_6$, Me_3NO, aq. CH_3CN.

and the subsequent incorporation of a diiron cluster. The peptide utilized, WASKLPSG, is derived from the N-terminal sequence of nickel-superoxide dismutase from *Streptomyces coelicolor*.[12] Previously, we employed this sequence to create an artificial 1,3-dithiol peptide coordinating a diiron-hexacarbonyl cluster.[9c] To synthesize the phosphine peptide, the desired eight residue peptide was first synthesized *via* solid-phase peptide synthesis using the Fmoc/*t*-Bu strategy. Lysine with an orthogonally protected amine group was selectively modified with diphenylphosphinopropionic acid to generate the iron-binding site. The side chain amine of tryptophan and the hydroxyl groups of the serines remain protected during the on-resin modification steps. Cleavage of the phosphine–peptide WASK(PPh_2)LPSG (**1a**) from the resin and reaction with [(μ-pdt)$Fe_2(CO)_6$; pdt = propane-1,3-dithiolate] produced the desired metallopeptide (μ-pdt)[Fe-$(CO)_3$][$Fe(CO)_2$WASK(PPh_2)-LPSG] (**1**). However, moderate sensitivity of the phosphines to oxidation reduced the overall yield. To prevent the loss of phosphine-peptide during synthesis and purification, an approach in which the free phosphine was replaced by a sulfur-protected phosphine synthon {3-(diphenylphosphorothioyl) propanoic acid} was evaluated (Scheme 2). After peptide cleavage from the resin, the phosphine sulfide was reduced by Raney™ nickel to produce the free phosphine-peptide which was immediately used, without further purification, for the reaction with (μ-pdt)$Fe_2(CO)_6$. Unfortunately, the use of sulfur-protected phosphine did not significantly improve the overall yield due to inefficiency of the desulfurization.

The metallopeptide was purified *via* HPLC, and a range of analytical techniques confirm the presence of the desired cluster (Fig. S1–S4†). Most importantly, the IR spectrum of the complex contains three characteristic bands at 2044, 1981, and 1925 cm^{-1} corresponding to the C–O stretching modes, similar to those observed for analogous monosubstituted diiron models.[4b,13] Furthermore, the ^{31}P NMR spectrum of the complex has a single resonance at 55.4 ppm, confirming formation of a unique complex with an Fe–P bond. Finally, ESI-MS provides further confirmation of the presence of an $Fe_2(CO)_5$ cluster.

Metallopeptides with unnatural amino acids. The necessity of including an orthogonally protected amino acid in the peptide sequence and carefully designing selective protection/deprotection steps limits the range of phosphines that can be employed using the synthetic scheme described above. Therefore, a second synthetic route in which an artificial phosphine amino acid is directly incorporated during solid-phase peptide synthesis was developed. This second method has the added benefit of shortening the side chain of the phosphine bearing amino acid. Since fewer rotamers are available, a more compact metal binding site with decreased solvent accessibility can be created. To demonstrate the utility of this strategy, using the method developed by Gilbertson *et al.*,[11b,14] three phosphine amino acids with different phosphine substituents were synthesized: *N*-Boc-3-(diethylphosphorothioyl)alanine (Boc-Epa-OH), *N*-Boc-3-(diisopropylphosphorothioyl)alanine (Boc-Ipa-OH), and *N*-Boc-3-(diphenylphosphorothioyl)alanine (Boc-Ppa-OH). Each was embedded into the tripeptide sequence, Val-Xpa-Leu (Xpa = unnatural phosphine amino acid) *via* solution phase peptide synthesis generating Val-Ppa-Leu, Val-Ipa-Leu, and Val-Epa-Leu (Scheme 3). Valine and leucine were chosen for hydrophobicity, to facilitate large-scale purification of the tripeptides on a normal-phase silica column. The peptides' N- and C-termini were protected as acetyl and methyl esters, respectively. Treatment of purified tripeptides with Raney™ nickel generated the free phosphines. Notably, ^{31}P NMR revealed that desulfurization also caused racemization at the α-carbon of the phosphine amino acid resulting in diasteromeric peptides. The phosphine peptides were metalated by reaction with (μ-pdt)$Fe_2(CO)_6$ or (μ-bdt)-$Fe_2(CO)_6$ (bdt = benzene-1,2-dithiolate) in CH_3CN/CH_2Cl_2 producing phosphine-substituted, diiron-peptide complexes as red solids in good yields. Four distinct complexes were prepared. Three complexes contain pdt as bridging ligand with variation of the phosphine substituents: [(Val-Epa-Leu)-{(μ-pdt)$Fe_2(CO)_5$}] (**2**), [(Val-Ipa-Leu)-{(μ-pdt)$Fe_2(CO)_5$}] (**3**), and [(Val-Ppa-Leu)-{(μ-pdt)$Fe_2(CO)_5$}] (**4**). A fourth complex, [(Val-Ppa-Leu)-{(μ-bdt)$Fe_2(CO)_5$}] (**5**), was synthesized using Val-Ppa-Leu as the ligand and bdt bridged diiron hexacarbonyl [(μ-bdt)$Fe_2(CO)_6$] as the metallo-precursor.

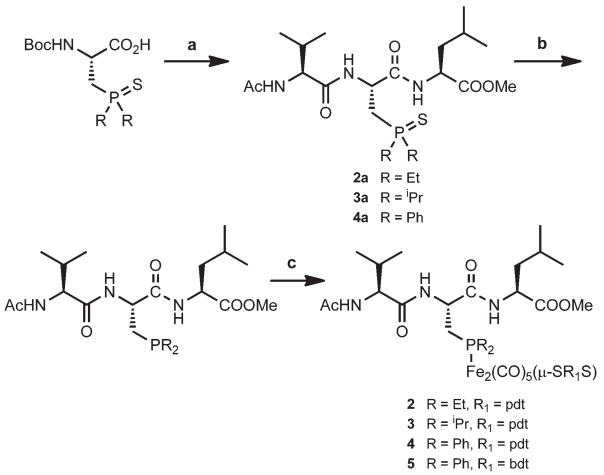

Scheme 3 Synthetic scheme for preparing diiron-tripeptide complexes with artificial *N*-Boc phosphine sulfide amino acids. Reaction conditions: (a) (i) H-Leu-OMe·HCl, PyBOP, DIEA, CH_2Cl_2, (ii) Ac-Val-OH, PyBOP, DIEA, CH_2Cl_2; (b) Raney™ nickel, CH_3CN, heat; (c) (μ-SR_1S)$Fe_2(CO)_6$, Me_3NO, CH_3CN.

Despite numerous attempts, X-ray quality crystals were not obtained for the diiron-peptide complexes. Thus, the compounds were characterized *via* spectroscopic and electrochemical methods. Spectroscopic data for **1–5** are summarized in Table 1. As shown in Fig. 1, the UV-vis spectra of the complexes in acetonitrile feature an Fe–S charge transfer band (CT) in the 340–370 nm region. Modifying the phosphine substituents but keeping the bridging ligand unchanged causes only a subtle shift in the wavelength of the charge transfer band. On the other hand, comparing the UV-vis spectra of **4** and **5** shows

Table 1 Wavelengths of the Fe–S charge transfer band (visible) and IR stretching frequencies in the ν(CO) region data for complexes **1–5**

Complex	λ_{max} (nm) (ε, M^{-1} cm^{-1})	ν_{CO}[b] (cm^{-1})
1[a]	350	2044 (s), 1981 (s), 1958 (sh), 1925 (w)
2	342 (9300)	2040 (s), 1981 (vs), 1966 (sh), 1921 (w)
3	351 (13 250)	2043 (s), 1979 (vs), 1960 (sh), 1919 (w)
4	354 (12 050)	2046 (s), 1984 (s), 1961 (sh), 1928 (w)
5	365 (25 700)	2053 (s), 1994 (s), 1937 (w)

[a] Extinction coefficient was not determined. [b] Intensity of the peaks: s = strong, vs = very strong, sh = shoulder, w = weak.

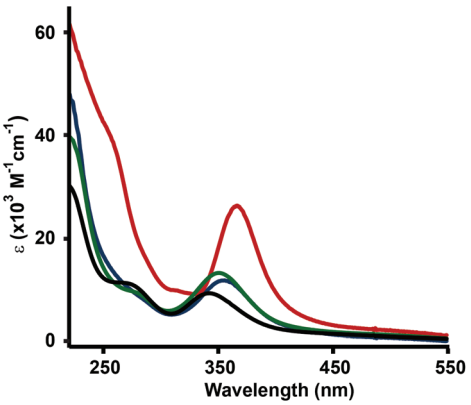

Fig. 1 UV-vis spectra of **2** (black), **3** (green), **4** (blue), and **5** (red) in acetonitrile. Spectra were obtained from solutions of approximately 0.1 mM complex.

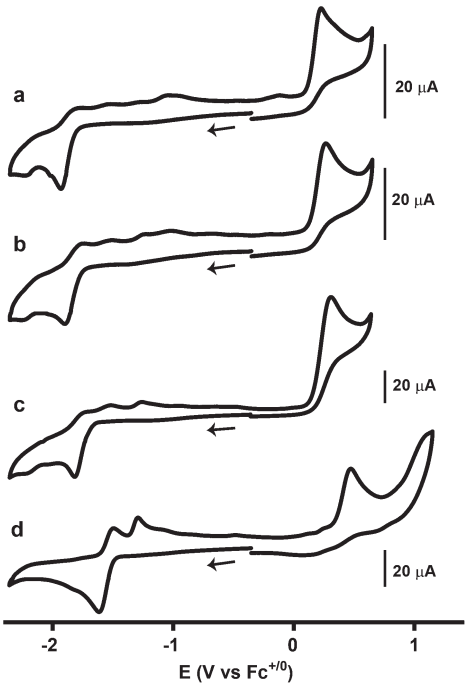

Fig. 2 Cyclic voltammograms of (a) **2** (0.88 mM), (b) **3** (0.69 mM), (c) **4** (1.39 mM), and (d) **5** (1 mM) in acetonitrile with 0.1 M $[NBu_4][PF_6]$ at a scan rate 0.2 V s^{-1}. Arrows mark the starting potential and scan direction.

that replacing pdt by bdt results in significant change in the position and intensity of the CT transition (Table 1).

FTIR spectra of the complexes show a characteristic three-band pattern in the C–O stretching region originating from the monosubstituted phosphine–$Fe_2(CO)_5$. The stretching frequencies of the carbonyls are a proxy for the electron density on the iron centers. As shown in Table 1, replacing aromatic groups on the phosphine with more electron donating alkyl groups (isopropyl or ethyl) results in a shift of the CO stretching frequencies by 5–6 cm^{-1} to lower wavenumbers. The weaker donor strength of bdt compared to pdt is also reflected in the higher C–O stretching frequencies observed for **5**.

Electrochemical studies in acetonitrile

Cyclic voltammetry demonstrates that the electrochemical properties of these complexes are similar to those reported for analogous monosubstituted diiron compounds. Cyclic voltammograms of the pdt complexes, **2**, **3** and **4**, feature an irreversible wave corresponding to Fe^IFe^I/Fe^IFe^0 reduction and an irreversible wave corresponding to Fe^IFe^I/Fe^IFe^{II} oxidation (Fig. 2 and Table 2). The irreversibility of the reduction suggests it is followed by a chemical reaction or, more specifically, decomposition of the complex. The reductively formed compound is potentially oxidizable, and this could explain the presence of several small oxidative waves in the oxidative scan following reduction. On the other hand, cyclic voltammograms of **5** show an irreversible oxidation wave at 0.47 V and a partially reversible reduction wave (i_p^{ox}/i_p^{red} = 0.47) at −1.62 V. As shown in Fig. 2, **5** also undergoes a second oxidation at *ca.* −1.29 V. This feature does not appear when the reductive scan is stopped prior to the reduction event, again suggesting an EC process in which the reduced species undergoes a chemical reaction forming a new species. Based on previous studies, we hypothesize that the chemical step following the reduction is probably slow exchange of a CO ligand with solvent to produce a phosphine/MeCN complex.[10b,15] The electrochemical behavior of **5** is very similar to that of analogous monosubstituted diiron-bdt-phosphine complexes recently reported by Pandey *et al.*[16] The reductive and oxidative peak potentials (E_p^{red} and E_p^{ox}, respectively) of the complexes correlate well with the donating abilities of the phosphines and the thiolates as deduced from their CO stretching frequencies. Among the pdt bridged complexes, the diphenylphosphino complex **4** is the most easily reduced. Changing the bridging thiolate from pdt to bdt has a more pronounced influence on the electronic properties of the diiron core as demonstrated by the 200 mV and 160 mV anodic shift of the Fe^IFe^I/Fe^IFe^0 and Fe^IFe^{II}/Fe^IFe^I couples, respectively, in **5** compared to **4**.

The ability of complexes **2–5** to electrocatalyze proton reduction from acetic acid was investigated in acetonitrile.

Table 2 Reduction potentials for **2–5** in acetonitrile and acetonitrile/water mixed solvents

	E_{pc} ($Fe^{I}Fe^{I}/Fe^{I}Fe^{0}$), V			E_{pa} ($Fe^{II}Fe^{I}/Fe^{I}Fe^{I}$), V		
Complex	CH_3CN	3 : 1 CH_3CN/H_2O	3 : 2 CH_3CN/H_2O	CH_3CN	3 : 1 CH_3CN/H_2O	3 : 2 CH_3CN/H_2O
2	−1.93	ND[a]	ND	+0.22	ND	ND
3	−1.90	−1.78	−1.74	+0.26	+0.22	+0.22
4	−1.82	−1.77	−1.72	+0.31	+0.29	+0.32
5	−1.62	−1.51	−1.47	+0.47	+0.48	+0.46

[a] ND = not determined.

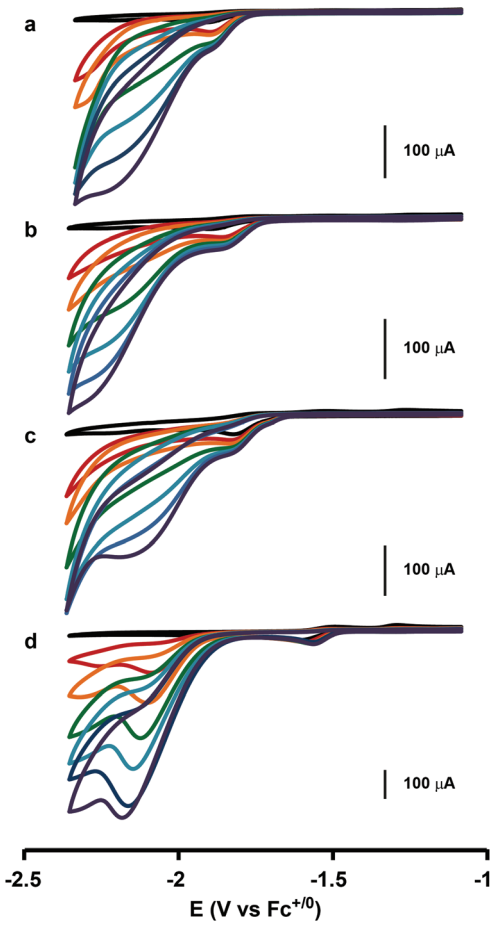

Fig. 3 Cyclic voltammograms of (a) **2** (0.88 mM), (b) **3** (0.69 mM), (c) **4** (1.39 mM), and (d) **5** (1 mM) in acetonitrile with various concentrations of acetic acid. The acid concentrations used are 5, 10, 20, 30, 40, and 50 mM. Reductive current increases with increasing acid concentration. Other experimental conditions are as described in Fig. 2.

To ensure that any observed electrocatalytic response was not a result of proton reduction by the glassy carbon electrode, control experiments without added catalyst were undertaken (Fig. S7 and S8†). For the complexes with a pdt bridge, sequential addition of AcOH resulted in increased reductive current corresponding to production of hydrogen (Fig. 3). Notably, this catalytic current is not observed at the $Fe^{I}Fe^{I}/Fe^{I}Fe^{0}$ reduction potential of the complexes (*ca.* −1.8 to −1.9 V). Instead, catalytic current is observed at more negative potentials in the range −2.1 to −2.3 V. Only a small enhancement of the peak current at the $Fe^{I}Fe^{I}/Fe^{I}Fe^{0}$ reduction potential is observed. This observation is consistent with the ECEC mechanism proposed in previous electrochemical studies of less electron rich analogues.[17] A likely explanation is that oxidative addition of a proton to the reduced $Fe^{I}Fe^{0}$ species forms the hydride $Fe^{I}Fe^{II}$-H, prompting subsequent displacement of CO by MeCN.[10b] The solvent-coordinated species is then reduced at more negative potential, leading to a negative shift in the potential at which catalytic current is observed (Fig. S5†). Compared to the pdt complexes, the bdt analogue, **5**, behaves slightly differently in the presence of acid. Addition of acetic acid renders the reduction peak of **5** completely irreversible with a small increase in peak current, but catalysis is observed only at a more negative potential, *ca.* −2.08 V. A similar ECEC mechanism is probably operative in which **5** undergoes reduction followed by protonation to form **5H**. The protonated species **5H** is then reduced at −2.08 V generating the electron rich $\mathbf{5H}^{-}$ which is basic enough to accept another proton. The catalytic cycle is then completed following reductive elimination of hydrogen. In light of possible concerns about heterogeneous catalysis, we performed a rinse test to confirm that no catalytically active species is deposited on the electrode. The result of this test is consistent with homogeneous catalysis (Fig. S6†).

Current enhancement observed in the presence of acetic acid is an indicator of the ability of the catalysts, and the ratio of the catalytic current (i_{cat}) to reductive peak current in the absence of acid (i_p) can be used as a marker to compare the performances of different complexes.[4a] A higher (i_{cat}/i_p) value indicates faster catalysis. To employ this analysis we determined peak currents (i_p) from the irreversible reduction waves of **2–5** in the absence of acid. Interestingly, at the highest acetic acid concentration (50 mM) investigated, **5** shows the largest current enhancement (i_{cat}/i_p = 23), **4** shows the least (i_{cat}/i_p = 6), and **2** and **3** show intermediate increases (i_{cat}/i_p = 18.5). However, relative to **4** and **5**, electrocatalysis by **2** and **3** occurs at more negative potentials [catalytic peak potential, E_p^{cat} = −2.30 V (**2** and **3**), −2.17 V (**4** and **5**)] due to the more electron-rich alkyl-phosphine substituents. The overpotentials

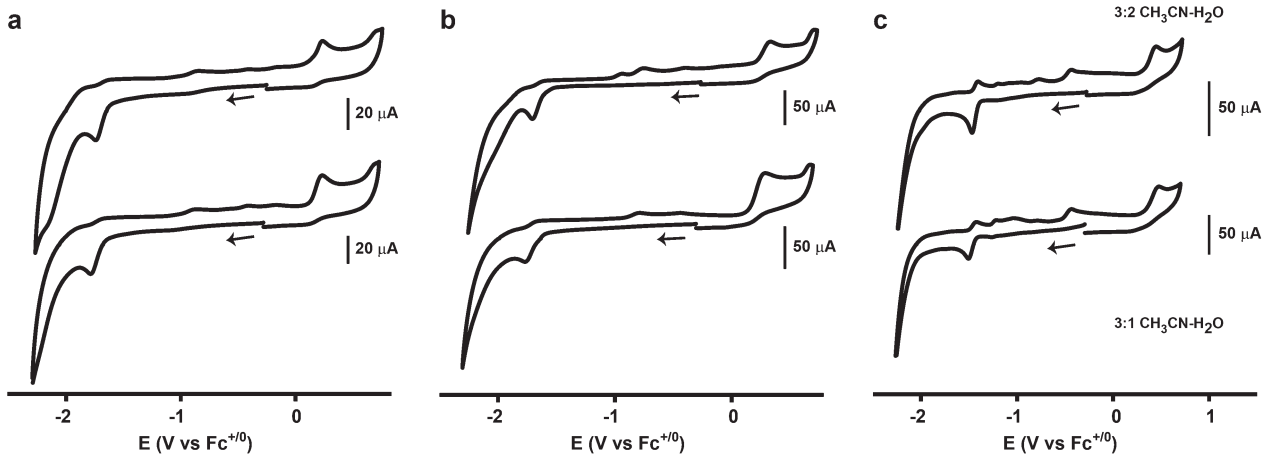

Fig. 4 Cyclic voltammograms of (a) **3**, (b) **4**, and (c) **5** in 3 : 2 acetonitrile-water (top) and 3 : 1 acetonitrile-water (bottom) at a potential scan rate of 0.2 V s^{-1}. In acetonitrile, 0.1 M $[NBu_4][PF_6]$ is used as supporting electrolyte. Similarly, 0.1 M KCl is used as the supporting electrolyte in water. The solvent mixtures include both electrolytes at the concentration formed by mixing. Concentrations of the complexes: (i) 3 : 1 CH_3CN/H_2O: **3** (0.63 mM), **4** (1.06 mM), and **5** (0.86 mM); (ii) 3 : 2 CH_3CN/H_2O: **3** (0.64 mM), **4** (1.25 mM), and **5** (0.72 mM).

for proton reduction by the four complexes, defined as the difference between the theoretical half-wave potential for reduction of the acid and the experimental half-wave potential for the catalytic process, were determined using the method reported by Artero and co-workers.[18] At the highest concentration of acetic acid (50 mM), all four complexes require relatively high overpotential for proton reduction (0.75–0.9 V). The overpotential requirement for the diphenylphosphino complexes (0.75 V for **4** and **5**) is slightly lower than that for the dialkylphosphino analogs (0.85 and 0.90 V for **2** and **3**, respectively).

Electrochemistry in acetonitrile/water mixtures

The improved water solubility of the diiron-peptide complexes relative to analogous diiron-phosphine complexes previously reported allowed electrocatalytic experiments in mixed acetonitrile-water solvents. Fig. 4 shows cyclic voltammograms from complexes **3**, **4**, and **5** in 3 : 1 and 3 : 2 CH_3CN/H_2O. The reduction potentials determined from these experiments are summarized in Table 2. Since the diethylphosphino complex (**2**) and the diisopropylphosphino complex (**3**) have similar electrochemical properties in acetonitrile, only **3** was studied in mixed solvents. The reductive wave associated with each of the Fe^IFe^I/Fe^IFe^0 couples shifts to less reducing potentials with increasing water content: shifts of 160, 100 and 150 mV for **3**, **4**, and **5**, respectively. Similar shifts were observed when electrochemical measurements of analogous diiron complexes with hydrophilic phosphine ligands, included to improve water solubility, were performed in mixed acetonitrile/water solvents.[15a,19] However, the $Fe^{II}Fe^I/Fe^IFe^I$ oxidation was virtually unaffected by water. This suggests that the reduction may be coupled to interaction of the reduced species with solvent.

Fig. 5 and 6 show electrocatalytic reduction of protons from AcOH by complexes **3–5** in CH_3CN/H_2O mixtures. Negative

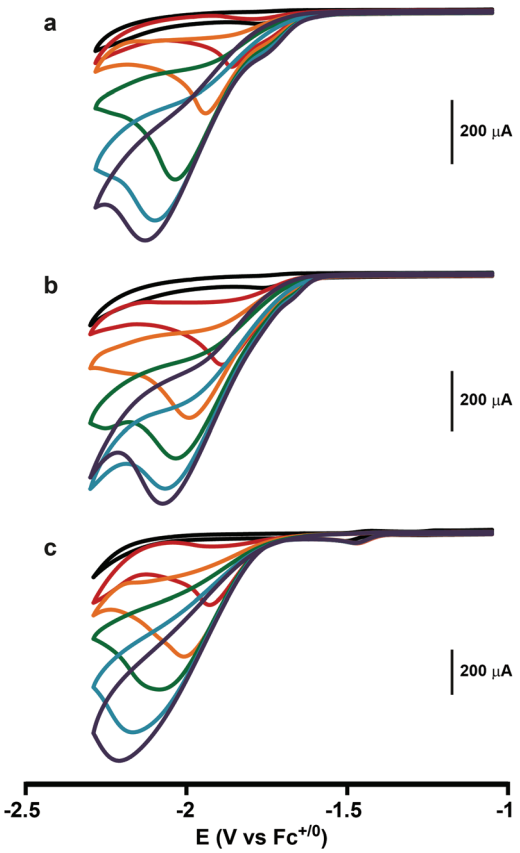

Fig. 5 Cyclic voltammograms of (a) **3** (0.63 mM), (b) **4** (1.06 mM), and (c) **5** (0.86 mM) in 3 : 1 acetonitrile-water with various concentrations of acetic acid. The acid concentrations used are 5, 10, 20, 30, 40, and 50 mM. Other experimental conditions are as described in Fig. 4.

control experiments without catalyst included clearly demonstrate that the electrocatalytic currents observed in the presence of catalyst are considerably higher than those from direct

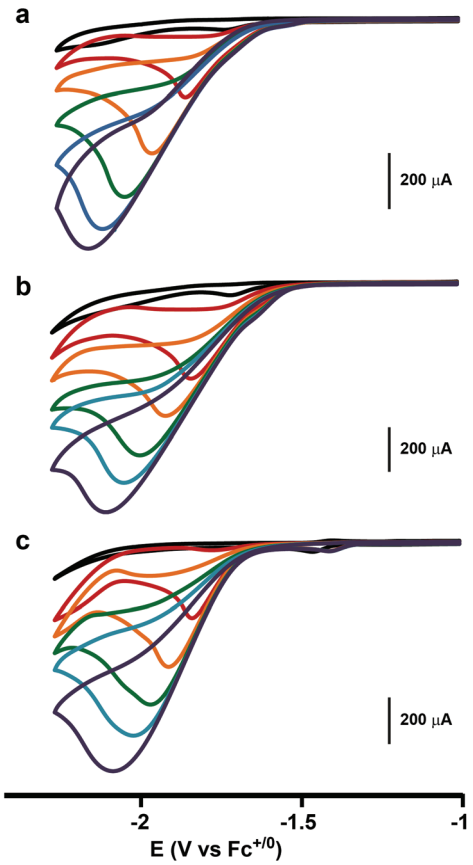

Fig. 6 Cyclic voltammograms of (a) **3** (0.64 mM), (b) **4** (1.25 mM), and (c) **5** (0.72 mM) in 3 : 2 acetonitrile-water with various concentrations of acetic acid. The acid concentrations used are 5, 10, 20, 30, 40, and 50 mM. Other experimental conditions are as described in Fig. 4.

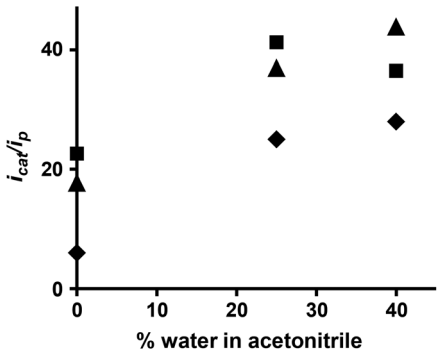

Fig. 7 Dependence of the (i_{cat}/i_p) on the amount of water present in the solvent: **3** (■), **4** (◆), **5** (▲). The TOFs are calculated from data shown in Fig. 3, 5 and 6.

reduction of protons by the electrode surface (Fig. S7 and S8†). For complexes **3** and **4**, there are notable changes in the intensities and positions of the catalytic waves when mixed aqueous solvents are used. Unlike the electrocatalysis in acetonitrile, cyclic voltammograms of **3** and **4** in CH_3CN/H_2O mixtures show catalysis at a potential very close to that of Fe^IFe^I/Fe^IFe^0 reduction. This is consistent with the hypothesis above that the catalytic waves in acetonitrile are associated with reduction of solvent-coordinated species. The presence of water likely significantly shifts the reduction potential of this solvent coordinated species (the second electrochemical step of the ECEC process) leading to a shift of the observed catalysis to more positive potentials. Furthermore, in 40% water, increasing the concentration of AcOH from 10 mM to 50 mM resulted in 19-fold and 21-fold enhancement of peak current for complexes **3** and **4**, respectively. In contrast, only 9-fold or 7-fold current increase was observed in neat acetonitrile. On the other hand, although the onset of catalysis by $\mathbf{5}^-$ also shifts to less reducing potentials with the addition of water, it is still significantly more negative than the $\mathbf{5}/\mathbf{5}^-$ reduction. To quantify the trends of electrocatalytic activities of **3–5** in the presence of water, Fig. 7 shows the dependence of the catalytic (i_{cat}/i_p) of **3**, **4**, and **5** in 50 mM acetic acid on the amount of water present. This shows that addition of water results in significant improvement in the catalytic activities of all three complexes. Similar improvement upon addition of water has been reported for Dubois-type nickel catalysts.[20] At such high water concentrations, the dielectric constant of the solution is significantly increased, and the acidity of the solution is also impacted. Either of these changes could lead to the enhanced catalytic current. Alternatively, faster proton transfer to the iron center facilitated by water could be another contributing factor. Additional experiments using different solvents and acids will be necessary to distinguish these possibilities. Finally, it should be noted that in the case of **5**, increasing the amount of water from 25% to 40% led to a slight drop in (i_{cat}/i_p). It is possible there is an optimal water concentration for catalysis by this complex, but the reason remains unclear.

Conclusions

In summary, we have demonstrated two synthetic schemes to introduce phosphines into peptides and to covalently anchor a $(\mu\text{-SRS})\{Fe(CO)_3\}\{Fe(CO)_2(PR_2R')\}$ cluster through the phosphine. This approach offers major advantages over other methods reported for building peptide-based diiron complexes: (1) the phosphine amino acids can be directly incorporated into designated peptide sequences; (2) electron-rich, stable diiron complexes can be prepared in only one step with peptide as the ligand resulting in better yields than syntheses requiring two peptide modifying steps; and (3) the synthesis of a diverse array of complexes can be achieved through variation of the artificial amino acid. Importantly, utilization of peptide ligands considerably increases the polarity of the complexes, allowing electrochemical studies in partially aqueous solvents. The presence of water has a significant influence on the electrochemical properties of the complexes as demonstrated by the shift of the reduction potential of the Fe^IFe^I/Fe^IFe^0 couple towards less reducing potentials and increased catalytic

currents. Thus the synthetic approach described here provides convenient access to monosubstituted diiron-peptide model complexes and opens the door for the design of more sophisticated peptides.

Experimental section

All reactions were carried out under an atmosphere of dry nitrogen using standard Schlenk and vacuum line techniques unless otherwise mentioned. Anhydrous solvents were purchased from Sigma-Aldrich, deuterated solvents from Cambridge Isotope Laboratories, and Fmoc protected amino acids and peptide coupling reagents from Protein Technologies. The compounds 3-(diphenylphosphino)-propionic acid,[21] *N*-Boc-3-iodo-alanine methyl ester,[22] *N*-Boc-3-(diphenylphosphorothioyl)-alanine (Boc-Ppa-OH),[14b] (μ-pdt)$Fe_2(CO)_6$,[23] and (μ-bdt)$Fe_2(CO)_6$ [24] were synthesized using literature procedures. The other *N*-Boc protected phosphine-sulfide amino acids (Boc-Epa-OH and Boc-Ipa-OH) were synthesized by slight modification of the literature method. All other starting materials were commercially available and used as received.

^{1}H, ^{13}C and ^{31}P NMR spectra were recorded at room temperature on a Varian NMR spectrometer (400 or 500 MHz for ^{1}H). NMR chemical shifts are quoted in ppm; spectra are referenced to tetramethylsilane for ^{1}H and ^{13}C NMR. Splitting patterns are designated as follows: s, singlet; d, doublet; t, triplet; m, multiplet; br, broad singlet; dd, doublet of doublets; td, triplet of doublets. FTIR spectra were recorded on a Bruker Vertex 70 spectrophotometer with MCT detector using a sealed liquid spectrophotometer cell with CaF_2 windows. UV-vis measurements were performed on a Hewlett-Packard 8453 spectrophotometer using quartz cuvettes with a 1 cm pathlength. MALDI-MS (matrix assisted laser desorption/ionization mass spectrometry) was performed on a Voyager DE STR using α-cyano-4-hydroxycinnamic acid as matrix. ESI-MS of metallopeptides with molecular weights above 1200 was performed using a Thermo Quantum Discovery Max triple-quadrupole mass spectrometer. Measurements were conducted in positive and negative ionization modes using a methanol/water (50 : 50 by volume) mobile phase at a flow rate of 10 mL min^{-1}. Mass spectra of lower molecular weight metallopeptides were recorded on a JEOL LCmate using atmospheric-pressure chemical ionization (APCI) in positive mode. HPLC purification of peptides was performed on a Waters 600E HPLC system. For analytical HPLC, a 3 × 50 mm C-18 column was used and for semi-preparative a PrepLC 25 mm module C-18 column.

3-(diphenylphosphorothioyl)propionic acid

3-(Diphenylphosphino)propionic acid (2.5 g, 9.7 mmol) and sulfur (0.316 g, 9.8 mmol) were suspended in toluene (17.5 mL) and refluxed under nitrogen for two hours. The reaction mixture was cooled to room temperature, and the toluene removed under reduced pressure to yield pure 3-(diphenylphosphorothioyl)propionic acid as a pale yellow solid (2.8 g, 99%). ^{1}H NMR (400 MHz, $CDCl_3$): δ = 7.83 (m, 4H, *Ph*), 7.5 (m, 6H, *Ph*), 2.73 (m, 4H, P–(CH_2)$_2$–COOH); ^{31}P{^{1}H} NMR (161.9 MHz, $CDCl_3$): δ = 41.9.

N-Boc-3-(diethylphosphorothioyl)-alanine methyl ester (Boc-Epa-OMe)

N-Boc phosphine sulfide methyl ester was synthesized from *N*-Boc-3-iodo-alanine methyl ester following the method previously described.[14b] Yield 63%. ^{1}H NMR (400 MHz, $CDCl_3$): δ = 5.68 (d, 1H, N*H*), 4.55–4.64 (m, 1H, N–C*H*–COO), 3.76 (s, 3H, COOCH_3), 2.52–2.64 (m, 2H, N–CH–CH_2–P), 2.02 (m, 4H, P–CH_2–CH_3), 1.42 (s, 9H, NH-*Boc*), 1.14–1.24 (m, 6H, P–CH_2–CH_3); ^{31}P{^{1}H} NMR (161.9 MHz, $CDCl_3$): δ = 52.8. R_f = 0.3 (35% EtOAc/hexane).

N-Boc-3-(diisopropylphosphorothioyl)-alanine methyl ester (Boc-Ipa-OMe)

This compound was prepared using the same strategy employed for Boc-Epa-OMe.[14b] Yield 69%. ^{1}H NMR (400 MHz, $CDCl_3$): δ = 5.86 (d, 1H, N*H*), 4.61–4.52 (m, 1H, N–C*H*–COO), 3.75 (s, 3H, COOCH_3), 2.38–2.46 (m, 2H, N–CH–CH_2–P), 2.13 (m, 2H, P-C*H*Me$_2$), 1.43 (s, 9H, NH-*Boc*), 1.15–1.24 (m, 12H, P-CH*Me*$_2$); ^{31}P{^{1}H} NMR (161.9 MHz, $CDCl_3$): δ = 64.7. R_f = 0.45 (40% EtOAc/hexane).

N-Boc-3-(diethylphosphorothioyl)-alanine (Boc-Epa-OH)

The amino acid was synthesized by the hydrolysis of the methyl ester following the literature procedure.[14b] Yield 82%. ^{1}H NMR (400 MHz, $CDCl_3$): δ = 9.54 (br, 1H, COO*H*), 5.87 (d, 1H, N*H*), 4.58–4.64 (m, 1H, N–C*H*–COO), 2.51 (m, 1H, N-CH-C*HH*′-P), 2.39 (m, 1H, N-CH-CH*H*′-P), 1.84–1.99 (m, 4H, P–CH_2–CH_3), 1.43 (s, 9H, NH-*Boc*), 1.13–1.22 (m, 6H, P–CH_2–CH_3); ^{13}C{^{1}H} NMR (100 MHz, $CDCl_3$): δ = 174.6 (s), 155.6 (s), 80.8 (s), 50 (s), 29.9 (d, J_{C-P} = 45 Hz), 24.72 (d, J_{C-P} = 51 Hz), 24.3 (d, J_{C-P} = 51 Hz), 6.26 (d, J_{C-P} = 5 Hz); ^{31}P{^{1}H} NMR (161.9 MHz, $CDCl_3$): δ = 51.6. R_f = 0.13 (1 : 1 EtOAc/hexane).

N-Boc-3-(diisopropylphosphorothioyl)-alanine (Boc-Ipa-OH)

This compound was also prepared using the procedure described by Greenfield *et al.*[14b] Yield 69%. ^{1}H NMR (400 MHz, $CDCl_3$): δ = 9.21 (br, 1H, COO*H*), 5.95 (d, 1H, N*H*), 4.56–4.62 (m, 1H, N–C*H*–COO), 2.42 (m, 1H, N–CH–C*HH*′–P), 2.32 (m, 1H, N–CH–CH*H*′–P), 2.09–2.21 (m, 2H, P-C*H*Me$_2$), 1.42 (s, 9H, NH-*Boc*), 1.15–1.27 (m, 12H, P-CH*Me*$_2$); ^{13}C{^{1}H} NMR (100 MHz, $CDCl_3$): δ = 171.1 (s), 155.4 (s), 80.6 (s), 50.4 (s), 28.7 (d, J_{C-P} = 49 Hz), 28.3 (d, J_{C-P} = 49 Hz), 25.5 (d, J_{C-P} = 48 Hz), 16.1 (m), 15.8 (m); ^{31}P{^{1}H} NMR (161.9 MHz, $CDCl_3$): δ = 65.1. R_f = 0.2 (1 : 1 EtOAc/hexane).

Solid phase peptide synthesis

The peptide WASKLPSG was synthesized on a Protein Technologies PS3 automated peptide synthesizer using the standard Fmoc/*t*-Bu protection strategy and HBTU as coupling reagent on Fmoc-Gly wang resin (Aapptec 0.54 mmol g^{-1}, 100–200 mesh) at 0.1 mmol scale. Following synthesis, the

peptide N-terminus was acetylated by treatment with 1 : 1 (v/v) acetic anhydride: *N*-methylmorpholine in DMF for 30 min.

On-resin modification of peptide

Resin-bound peptide (0.05 mmol) was treated with 2% hydrazine (v/v) in DMF (10 mL) for 1 h under nitrogen at room temperature. The resin beads were then thoroughly washed with DMF. The resin beads were then treated with a solution of 3-(diphenylphosphino)propionic acid or 3-(diphenylphosphorothioyl)propionic acid (0.15 mmol) together with HATU (1-[bis(dimethylamino)methylene]-1*H*-1,2,3-triazolo[4,5-*b*]pyridinium 3-oxid hexafluorophosphate) (54 mg, 0.14 mmol) and *N*,*N*-diisopropylethylamine (DIEA) (30 μL, 0.16 mmol) in 8 mL DMF for 45 min. The coupling was repeated a second time to ensure complete reaction. The resin was washed with DMF (4 × 2 mL) and dichloromethane (5 × 2 mL) followed by cleavage of the peptide using 95 : 2.5 : 2.5 TFA/water/TIPS (v/v) for two hours (TFA = trifluoroacetic acid, TIPS = triisopropylsilane). After concentrating the TFA solution, the peptide was precipitated with diethyl ether at −20 °C and purified by reverse phase HPLC using aqueous acetonitrile gradients containing 0.1% TFA (v/v). General yields of the peptides after purification were *ca.* 20%.

Peptide WASK{–$COC_2H_4PPh_2$}LPSG, 1a. $^{31}P\{^1H\}$ NMR (161.9 MHz, CD_3CN): δ = −14.4; R_t = 60 min (59% acetonitrile, flow rate: 0.5 mL min^{-1}); MALDI-TOF MS: *m*/*z* = 1149.8 $(M + Na)^+$.

Peptide WASK{–$COC_2H_4P(S)Ph_2$}LPSG. $^{31}P\{^1H\}$ NMR (161.9 MHz, CD_3CN): δ = 43.08; R_t = 54 min (53.6% acetonitrile, flow rate: 0.5 mL min^{-1}); MALDI-TOF MS: *m*/*z* = 1181.6 $(M + Na)^+$.

Solution phase peptide synthesis

N-Boc protected phosphino amino acid (1 equiv.), leucine methyl ester hydrochloride (1 equiv.), and PyBOP {(Benzotriazol-1-yloxy)tripyrrolidinophosphonium hexafluorophosphate} (1.5 equiv.) were dissolved in CH_2Cl_2 under nitrogen and cooled to 0 °C. DIEA (3 equiv.) was added, and the reaction mix was allowed to warm to room temperature. After stirring at room temperature for 40 min, the reaction mixture was washed with 1 M HCl, saturated $NaHCO_3$, and brine. The CH_2Cl_2 solution was dried over $MgSO_4$, filtered, concentrated under reduced pressure, and purified over silica using hexane/ethyl acetate as eluent. The *N*-Boc methyl ester protected dipeptide was treated with 1 : 1 TFA/CH_2Cl_2 until complete removal of Boc was indicated by TLC. The reaction mixture was then concentrated under reduced pressure, dissolved in toluene and concentrated until white solid was obtained. That solid was dissolved in CH_2Cl_2 and concentrated followed by drying under vacuum for 12 h. The *N*-acetyl valine (1 equiv.) was then coupled to the TFA salt of the dipeptide using the same procedure to the point of the brine washing. The CH_2Cl_2 solution containing tripeptide was dried, concentrated and purified over silica using 2% methanol/ethyl acetate as eluent.

Ac-Val-Epa-Leu-OMe (2a). ^1H NMR (400 MHz, $CDCl_3$): δ = 7.98 (d, 1H, N*H*), 7.82 (d, 1H, N*H*), 6.06 (m, 1H, N*H*), 4.89 (m, 1H, N–C*H*–CO), 4.44 (m, 1H, N–C*H*–CO), 4.12–4.22 (m, 1H, N–C*H*–CO), 3.69 (s, 3H, $COOCH_3$), 2.1–2.5 (m, 3H, Epa: N–CH–CH_2–P, Val: CH–C*H*Me_2), 2.06 (s, 3H, NH-$COCH_3$), 1.7–1.94 (m, 6H, Epa: P–CH_2–CH_3, Leu: N–CH–CH_2–$CHMe_2$), 1.37 (m, 1H, Leu: CH_2–C*H*Me_2), 1.11–1.21 (m, 6H, P–CH_2–CH_3), 0.89–0.95 (m, 12H, Leu: CH_2–CH*Me*$_2$, Val: CH–CH*Me*$_2$); $^{31}P\{^1H\}$ NMR (161.9 MHz, $CDCl_3$): δ = 52.0 (major isomer 92%), 51.9 (minor diastereomer 8%); R_f = 0.2 (EtOAc); MALDI-TOF MS: *m*/*z* = 500.31 $(M + Na)^+$. The two diastereomeric tripeptides could not be separated because of nearly identical polarity.

Ac-Val-Ipa-Leu-OMe (3a). ^1H NMR (400 MHz, $CDCl_3$): δ = 7.94 (d, 1H, N*H*), 7.85 (d, 1H, N*H*), 6.04 (m, 1H, N*H*), 4.88 (m, 1H, N–C*H*–CO), 4.45 (m, 1H, N–C*H*–CO), 4.28 (m, 1H, N–C*H*–CO), 3.72 (s, 3H, $COOCH_3$), 2.11–2.48 (m, 5H, Ipa: βH and P–C*H*Me_2, Val: βH), 2.09 (s, 3H, NH–$COCH_3$), 1.63–1.78 (m, 3H, Leu: βH and γH), 1.19–1.31 (m, 12H, P-CH*Me*$_2$), 0.92–1 (m, 12H, Leu: CH_2–CH*Me*$_2$, Val: CH–CH*Me*$_2$); $^{31}P\{^1H\}$ NMR (161.9 MHz, $CDCl_3$): δ = 65.0. R_f = 0.22 (EtOAc). MALDI-TOF MS: *m*/*z* = 528.36 $(M + Na)^+$.

Ac-Val-Ppa-Leu-OMe (4a). ^1H NMR (400 MHz, CD_2Cl_2): δ = 7.83 (m, 4H, P–*Ph*), 7.75 (d, 1H, N*H*), 7.49 (m, 6H, P–*Ph*), 7.10 (d, 1H, N*H*), 5.98 (d, 1H, N*H*), 4.69–4.79 (m, 1H, N–C*H*–CO), 4.21 (m, 1H, N–C*H*–CO), 4.07 (m, 1H, N–C*H*–CO), 3.64 (s, 3H, $COOCH_3$), 3.14 (m, 2H, Ppa: βH), 2.09 (m, 1H, Val: βH), 2.06 (s, 3H, NH-$COCH_3$), 1.52–1.54 (m, 3H, Leu: βH and γH), 0.81–0.90 (m, 12 H, Leu: CH_2–CH*Me*$_2$, Val: CH–CH*Me*$_2$); $^{31}P\{^1H\}$ NMR (161.9 MHz, CD_2Cl_2): δ = 40.35. R_f = 0.1 (2 : 1 EtOAc/hexane). MALDI-TOF MS: *m*/*z* = 595.8 $(M + Na)^+$.

Desulfurization of WASK{–$COC_2H_4P(S)Ph_2$}LPSG

Raney™ nickel slurry (800 mg) was transferred to a Schlenk flask and washed with deaerated methanol until the washings were clear followed by washing with CH_3CN (3 × 5 mL). The peptide (29 μmol) in 4 : 1 CH_3CN/water (v/v, 10 mL) was added to the Raney™ nickel and stirred at room temperature for 2 h. Completion of desulfurization was confirmed by MALDI-TOF MS. The Raney™ nickel was allowed to settle, and the reaction mixture was filtered into a Schlenk flask under an argon atmosphere. The Raney™ nickel was rinsed with 5 × 5 mL CH_3CN and filtered into the Schlenk flask. The CH_3CN solution was concentrated under reduced pressure and lyophilized overnight to obtain phosphine-peptide (**1a**) as white powder that was immediately used for the cluster incorporation.

Synthesis of 1 from 1a

The phosphine-peptide **1a** (3 μmol) was dissolved in CH_3CN (5 mL). In a separate flask, (μ-pdt)$Fe_2(CO)_6$ (4 mg) and trimethylamine-*N*-oxide (2 mg) were dissolved in CH_3CN (1 mL) and stirred in the dark for 10 min. This solution was transferred *via* cannula to the peptide solution. After stirring for two hours in the dark, the solvent was removed under reduced pressure, and the product metallopeptide (**1**) was purified *via* reverse phase HPLC. Yield 15%. $^{31}P\{^1H\}$ NMR (161.9 MHz, 10% D_2O/CD_3CN): δ = 55.43. IR (KBr, cm^{-1}): ν(CO) = 2044, 1981, 1958, 1925. ESI-MS: (EI^+) *m*/*z* = 1458.5 $(M + H - CO)^+$; (EI^-) *m*/*z* = 1456.4 $(M–H–CO)^-$, 1373.6 $(M–H–4CO)^-$. R_t =

76 min (73.4% acetonitrile, flow rate 0.5 mL min^{-1}). The extinction coefficient of the complex was not determined due to difficulty obtaining an accurate concentration value for solutions. Determination of the concentration of **1a** from 280 nm absorbance of tryptophan is not possible due to overlap of the 280 and 350 nm bands.

Desulfurization of tripeptides (2a, 3a, 4a)

To a slurry of Raney™ nickel (washed with deaerated MeOH and CH_3CN) was added a solution of tripeptide (0.25 mmol) in CH_3CN (15 mL). The reaction mixture was stirred at 45–55 °C under argon until complete reduction of the phosphine sulfide as indicated by either ^{31}P NMR or MALDI. The Raney™ nickel was allowed to settle, and the supernatant was filtered under argon. The filtrate was concentrated under reduced pressure and lyophilized overnight. The phosphine tripeptide was immediately used for the reaction with diiron hexacarbonyl precursor.

Reduction of 2a. Reaction condition: 2 h at 25 °C, then 1 h at 44 °C. MALDI-TOF MS: m/z = 446.37 $(M + H)^+$.

Reduction of 3a. Reaction condition: 4 h at 48 °C. $^{31}P\{^1H\}$ NMR (161.9 MHz, $CDCl_3$): δ = −4.1.

Reduction of 3a. Reaction condition: 4 h at 55 °C. $^{31}P\{^1H\}$ NMR (161.9 MHz, $CDCl_3$): δ = −23.3.

General procedure for cluster incorporation into tripeptide

A solution of (μ-SRS)$Fe_2(CO)_6$ (0.3 mmol) (R = pdt or bdt) in CH_3CN (3 mL) was added dropwise to a CH_2Cl_2 (2 mL) solution of $Me_3NO{\cdot}2H_2O$ (0.3 mmol) at room temperature. After stirring the reaction mixture in the dark for 10 min, phosphine peptide (0.2 mmol) in CH_2Cl_2 (10 mL) was added dropwise. After 3 h, the solvent was removed under reduced pressure, and the residue was purified by silica gel chromatography with 2% MeOH/CH_2Cl_2 to produce the peptide-diiron complex as red powder.

(Val-Epa-Leu)-{(μ-pdt)$Fe_2(CO)_5$} (2). Yield 77%. ^1H NMR (400 MHz, CD_2Cl_2): δ = 6.78 (d, 1H, N*H*), 6.63 (d, 1H, N*H*), 5.98 (d, 1H, N*H*), 4.93 (m, 1H, N–C*H*–CO), 4.47 (m, 1H, N–C*H*–CO), 4.18 (m, 1H, N–C*H*–CO), 3.69 (s, 3H, NH–COCH_3), 2.1–2.56 (m, 5H, Epa: βH, Val: βH, pdt: S–C*HH′*), 1.99 (s, 3H, NH–COCH_3), 1.72–1.88 (m, 6H, Epa: P–CH_2–CH_3, pdt: S–C*HH′*) 1.56–1.60 (m, 5H, Leu: βH and γH, pdt: CH_2–CH_2–CH_2), 1.23–1.26 (m, 6H, P–CH_2–CH_3), 0.90–0.94 (m, 12H, Leu: CH_2–CHMe_2, Val: CH–CHMe_2); $^{31}P\{^1H\}$ NMR (161.9 MHz, CD_2Cl_2): δ = 54.8 (major isomer 78%), 54.9 (minor diastereomer 22%); IR (CH_2Cl_2, cm^{-1}): ν(CO) = 2040, 1981, 1966, 1921; R_f = 0.5 (EtOAc); MS $(APCI^+)$: m/z = 804.1117 (calculated 804.1139).

(Val-Ipa-Leu)-{(μ-pdt)$Fe_2(CO)_5$} (3). Yield 80%. ^1H NMR (400 MHz, CD_2Cl_2): δ = 6.85 (d, 1H, N*H*), 6.63 (d, 1H, N*H*), 5.95 (d, 1H, N*H*), 4.98 (m, 1H, N–C*H*–CO), 4.47 (m, 1H, N–C*H*–CO), 4.03–4.18 (m, 1H, N–C*H*–CO), 3.67 (s, 3H, COOCH_3), 1.97–2.24 (m, 12H, Leu: COOCH_3, Ipa: βH and PC*H*Me_2, Val: βH, pdt: SCH_2), 1.55–1.68 (m, 7H, Leu: βH and γH, pdt: CH_2–CH_2–CH_2), 1.26–1.35 (m, 12H, Ipa: P–CHMe_2), 0.89–0.98 (m, 12H, Leu: CH_2–CHMe_2, Val: CH–CHMe_2); $^{31}P\{^1H\}$ NMR (161.9 MHz, CD_2Cl_2): δ = 70.2 (major isomer 60%), 69.8 (minor diastereomer 40%); IR (CH_2Cl_2, cm^{-1}): ν(CO) = 2043, 1979, 1960, 1919; R_f = 0.6 (EtOAc); MS $(APCI^+)$: m/z = 832.1449 (calculated 832.1452).

(Val-Ppa-Leu)-{(μ-pdt)$Fe_2(CO)_5$} (4). Yield 87%. ^1H NMR (400 MHz, CD_2Cl_2): δ = 7.62–7.76 (m, 4H, P–*Ph*), 7.41–7.51 (m, 6H, P–*Ph*), 6.56 (d, 1H, N*H*), 5.77 (d, 1H, N*H*), 5.52 (d, 1H, N*H*), 4.74 (m, 1H, N–C*H*–CO), 4.36 (m, 1H, N–C*H*–CO), 3.75 (m, 1H, N–C*H*–CO), 3.69 (s, 3H, COOCH_3), 2.83–3.30 (m, 2H, Ppa: P–CH_2), 1.93 (s, 3H, NH-COCH_3), 1.85 (m, 5H, Val: βH, pdt: SCH_2), 1.50–1.58 (m, 6H, Leu: βH and γH, pdt: CH_2–CH_2–CH_2), 0.73–0.85 (m, 12H, Leu: CH_2–CHMe_2, Val: CH–CHMe_2); $^{31}P\{^1H\}$ NMR (161.9 MHz, CD_2Cl_2): δ = 55.3 (major isomer 70%), 55.9 (minor diastereomer, 30%); IR (CH_2Cl_2, cm^{-1}): ν(CO) = 2046, 1984, 1961, 1928; R_f = 0.3 (2% MeOH/CH_2Cl_2); MS $(APCI^+)$: m/z = 900.1159 (calculated 900.1139).

(Val-Ppa-Leu)-{(μ-bdt)$Fe_2(CO)_5$} (5). Yield 84%. ^1H NMR (400 MHz, CD_2Cl_2): δ = 7.65 (m, 2H, bdt), 7.47–7.53 (m, 4H, P–*Ph*), 7.32–7.4 (m, 2H, P–*Ph*), 7.24–7.27 (4H, P–*Ph*), 6.94 (d, 1H, N*H*), 6.54 (d, 1H, N*H*), 6.48 (td, 1H, bdt), 6.39 (m, 1H, bdt), 4.84 (m, 1H, N–C*H*–CO), 4.41 (m, 1H, N–C*H*–CO), 3.73 (s, 3H, COOCH_3), 3.7 (m, 1H, N–C*H*–CO), 2.73 (m, 2H, Ppa: PCH_2), 1.94 (s, 3H, NH–COCH_3), 1.49–1.60 (m, 4H, Leu: βH and γH, Val: βH), 0.72–0.90 (m, 12H, Leu: CH_2–CHMe_2, Val: CH–CHMe_2); $^{31}P\{^1H\}$ NMR (161.9 MHz, CD_2Cl_2): δ = 51.3; IR (CH_2Cl_2, cm^{-1}): ν(CO) = 2053, 1994, 1937; R_f = 0.37 (2% MeOH/CH_2Cl_2); MS $(APCI^+)$: m/z = 934.0973 (calculated 934.0983).

Electrochemistry

Electrochemical measurements were made using a CHI 1200A electrochemical analyzer under an atmosphere of argon. A conventional three-electrode cell was used. The working electrode was a 3 mm diameter glassy carbon disk polished successively with 1 mm and 0.3 mm deagglomerated alpha alumina and sonicated for 15 min in ultrapure water prior to use. The Ag/Ag^+ reference electrode was prepared by immersing a silver wire anodized with AgCl in an CH_3CN solution of 0.1 M $[NBu_4][PF_6]$. A platinum wire was used as counter electrode. For electrochemical studies in CH_3CN, a 0.1 M solution of $[NBu_4][PF_6]$ was used as supporting electrolyte. Mixtures of 0.1 M $[NBu_4][PF_6]$ in CH_3CN and 0.1 M KCl in water were used for mixed solvent experiments. Argon was sparged through the solution for 15 min before experiments and anaerobicity was maintained during the electrochemical measurements by an atmosphere of argon. All potentials are reported relative to the ferrocene couple (Fc^+/Fc). Concentrations of the complexes were determined spectrophotometrically using the extinction coefficients of the Fe–S charge transfer bands.

The catalytic activities of the complexes were compared using the ratio (i_{cat}/i_p) instead of turnover frequencies (TOF) because determination of TOF is difficult without additional mechanistic information. Since catalysis occurs at a potential more negative than that of the Fe^IFe^I/Fe^IFe^0 couple and likely involves solvent-substituted complex, the potential of this second reduction process in the absence of acid is unknown. Therefore, application of 'foot-of-the-wave' analysis is also not appropriate for these voltammograms.

Acknowledgements

This research was supported through the Center for Bio-Inspired Solar Fuel Production, an Energy Frontier Research Center funded by the U.S. Department of Energy, Office of Science, Office of Basic Energy Sciences under Award Number 770 DE-SC0001016.

References

1 (*a*) M. W. W. Adams and E. I. Stiefel, *Science*, 1998, **282**, 1842–1843; (*b*) M. Frey, *ChemBioChem*, 2002, **3**, 153–160; (*c*) J. C. Fontecilla-Camps, A. Volbeda, C. Cavazza and Y. Nicolet, *Chem. Rev.*, 2007, **107**, 4273–4303.

2 (*a*) J. W. Peters, W. N. Lanzilotta, B. J. Lemon and L. C. Seefeldt, *Science*, 1998, **282**, 1853–1858; (*b*) Y. Nicolet, C. Piras, P. Legrand, C. E. Hatchikian and J. C. Fontecilla-Camps, *Structure*, 1999, **7**, 13–23.

3 (*a*) D. J. Evans and C. J. Pickett, *Chem. Soc. Rev.*, 2003, **32**, 268–275; (*b*) T. R. Simmons, G. Berggren, M. Bacchi, M. Fontecave and V. Artero, *Coord. Chem. Rev.*, 2014, **270–271**, 127–150.

4 (*a*) G. A. N. Felton, C. A. Mebi, B. J. Petro, A. K. Vannucci, D. H. Evans, R. S. Glass and D. L. Lichtenberger, *J. Organomet. Chem.*, 2009, **694**, 2681–2699; (*b*) C. Tard and C. J. Pickett, *Chem. Rev.*, 2009, **109**, 2245–2274.

5 (*a*) G. Berggren, A. Adamska, C. Lambertz, T. R. Simmons, J. Esselborn, M. Atta, S. Gambarelli, J. M. Mouesca, E. Reijerse, W. Lubitz, T. Happe, V. Artero and M. Fontecave, *Nature*, 2013, **499**, 66–69; (*b*) J. Esselborn, C. Lambertz, A. Adamska-Venkatesh, T. Simmons, G. Berggren, J. Noth, J. Siebel, A. Hemschemeier, V. Artero, E. Reijerse, M. Fontecave, W. Lubitz and T. Happe, *Nat. Chem. Biol*, 2013, **9**, 607–609; (*c*) W. K. Myers, T. A. Stich, D. L. M. Suess, J. M. Kuchenreuther, J. R. Swartz and R. D. Britt, *J. Am. Chem. Soc.*, 2014, **136**, 12237–12240.

6 (*a*) R. D. Bethel and M. Y. Darensbourg, *Nature*, 2013, **499**, 40–41; (*b*) S. Roy and A. K. Jones, *Nat. Chem. Biol*, 2013, **9**, 603–605.

7 (*a*) X. de Hatten, E. Bothe, K. Merz, I. Huc and N. Metzler-Nolte, *Eur. J. Inorg. Chem.*, 2008, **2008**, 4530–4537; (*b*) W. J. Shaw, *Catal. Rev.: Sci. Eng.*, 2012, **54**, 489–550; (*c*) B. Ginovska-Pangovska, A. Dutta, M. L. Reback, J. C. Linehan and W. J. Shaw, *Acc. Chem. Res.*, 2014, **47**, 2621–2630; (*d*) G. Caserta, S. Roy, M. Atta, V. Artero and M. Fontecave, *Curr. Opin. Chem. Biol.*, 2015, **25**, 36–47.

8 (*a*) M. Faiella, C. Andreozzi, R. T. M. de Rosales, V. Pavone, O. Maglio, F. Nastri, W. F. DeGrado and A. Lombardi, *Nat. Chem. Biol*, 2009, **5**, 882–884; (*b*) V. Nanda and R. L. Koder, *Nat. Chem.*, 2010, **2**, 15–24; (*c*) D. W. Watkins, C. T. Armstrong and J. L. R. Anderson, *Curr. Opin. Chem. Biol.*, 2014, **19**, 90–98; (*d*) F. Yu, V. M. Cangelosi, M. L. Zastrow, M. Tegoni, J. S. Plegaria, A. G. Tebo, C. S. Mocny, L. Ruckthong, H. Qayyum and V. L. Pecoraro, *Chem. Rev.*, 2014, **114**, 3495–3578.

9 (*a*) A. K. Jones, B. R. Lichtenstein, A. Dutta, G. Gordon and P. L. Dutton, *J. Am. Chem. Soc.*, 2007, **129**, 14844–14845; (*b*) U.-P. Apfel, M. Rudolph, C. Apfel, C. Robl, D. Langenegger, D. Hoyer, B. Jaun, M.-O. Ebert, T. Alpermann, D. Seebach and W. Weigand, *Dalton Trans.*, 2010, **39**, 3065–3071; (*c*) S. Roy, S. Shinde, G. A. Hamilton, H. E. Hartnett and A. K. Jones, *Eur. J. Inorg. Chem.*, 2011, **2011**, 1050–1055; (*d*) A. Roy, C. Madden and G. Ghirlanda, *Chem. Commun.*, 2012, **48**, 9816–9818.

10 (*a*) F. Gloaguen, J. D. Lawrence and T. B. Rauchfuss, *J. Am. Chem. Soc.*, 2001, **123**, 9476–9477; (*b*) D. S. Chong, I. P. Georgakaki, R. Mejia-Rodriguez, J. Samabria-Chinchilla, M. P. Soriaga and M. Y. Darensbourg, *Dalton Trans.*, 2003, 4158–4163.

11 (*a*) S. R. Gilbertson, G. H. Chen and M. McLoughlin, *J. Am. Chem. Soc.*, 1994, **116**, 4481–4482; (*b*) A. Agarkov, S. Greenfield, D. Xie, R. Pawlick, G. Starkey and S. R. Gilbertson, *Biopolymers*, 2006, **84**, 48–73.

12 J. Shearer and L. M. Long, *Inorg. Chem.*, 2006, **45**, 2358–2360.

13 L.-C. Song, H.-T. Wang, J.-H. Ge, S.-Z. Mei, J. Gao, L.-X. Wang, B. Gai, L.-Q. Zhao, J. Yan and Y.-Z. Wang, *Organometallics*, 2008, **27**, 1409–1416.

14 (*a*) S. R. Gilbertson, S. E. Collibee and A. Agarkov, *J. Am. Chem. Soc.*, 2000, **122**, 6522–6523; (*b*) S. J. Greenfield, A. Agarkov and S. R. Gilbertson, *Org. Lett.*, 2003, **5**, 3069–3072.

15 (*a*) R. Mejia-Rodriguez, D. Chong, J. H. Reibenspies, M. P. Soriaga and M. Y. Darensbourg, *J. Am. Chem. Soc.*, 2004, **126**, 12004–12014; (*b*) F. Gloaguen, D. Morvan, J.-F. Capon, P. Schollhammer and J. Talarmin, *J. Electroanal. Chem.*, 2007, **603**, 15–20.

16 I. K. Pandey, S. M. Mobin, N. Deibel, B. Sarkar and S. Kaur-Ghumaan, *Eur. J. Inorg. Chem.*, 2015, **2015**, 2875–2882.

17 (*a*) J.-F. Capon, S. Ezzaher, F. Gloaguen, F. Y. Petillon, P. Schollhammer, J. Talarmin, T. J. Davin, J. E. McGrady and K. W. Muir, *New J. Chem.*, 2007, **31**, 2052–2064; (*b*) J.-F. Capon, F. Gloaguen, F. Y. Petillon, P. Schollhammer and J. Talarmin, *Coord. Chem. Rev.*, 2009, **253**, 1476–1494; (*c*) P. Surawatanawong, J. W. Tye, M. Y. Darensbourg and M. B. Hall, *Dalton Trans.*, 2010, **39**, 3093–3104.

18 V. Fourmond, P.-A. Jacques, M. Fontecave and V. Artero, *Inorg. Chem.*, 2010, **49**, 10338–10347.

19 Y. Na, M. Wang, K. Jin, R. Zhang and L. Sun, *J. Organomet. Chem.*, 2006, **691**, 5045–5051.

20 (*a*) A. Jain, S. Lense, J. C. Linehan, S. Raugei, H. Cho, D. L. DuBois and W. J. Shaw, *Inorg. Chem.*, 2011, **50**, 4073–4085; (*b*) U. J. Kilgore, J. A. S. Roberts, D. H. Pool, A. M. Appel, M. P. Stewart, M. R. DuBois, W. G. Dougherty, W. S. Kassel, R. M. Bullock and D. L. DuBois, *J. Am. Chem. Soc.*, 2011, **133**, 5861–5872; (*c*) M.-H. Ho, M. O'Hagan, M. Dupuis, D. L. DuBois, R. M. Bullock, W. J. Shaw and S. Raugei, *Dalton Trans.*, 2015, **44**, 10969–10979;

(*d*) W. A. Hoffert, J. A. S. Roberts, R. Morris Bullock and M. L. Helm, *Chem. Commun.*, 2013, **49**, 7767–7769; (*e*) J. Hou, M. Fang, A. J. P. Cardenas, W. J. Shaw, M. L. Helm, R. M. Bullock, J. A. S. Roberts and M. O'Hagan, *Energy Environ. Sci.*, 2014, **7**, 4013–4017.

21 E. N. Tsvetkov, N. A. Bondarenko, I. G. Malakhova and M. I. Kabachnik, *Synthesis*, 1986, 198–208.

22 S. van Zutphen, V. J. Margarit, G. Mora and P. Le Floch, *Tetrahedron Lett.*, 2007, **48**, 2857–2859.

23 E. J. Lyon, I. P. Georgakaki, J. H. Reibenspies and M. Y. Darensbourg, *Angew. Chem., Int. Ed.*, 1999, **38**, 3178–3180.

24 J. Zhao, Z. Wei, X. Zeng and X. Liu, *Dalton Trans.*, 2012, **41**, 11125–11133.